Available online at www.sciencedirect.com
ScienceDirect
Measurement 41 (2008) 471–480
Measurement
www.elsevier.com/locate/measurement

# Measurement and simulation of the voltage distribution and the electric field on a glass insulator string

V.T. Kontargyri *, L.N. Plati, I.F. Gonos, I.A. Stathopulos

*School of Electrical and Computer Engineering, Electric Power Department, High Voltage Laboratory, 9, Iroon Politechniou Street, 15780 Zografou, Athens, Greece*

Received 16 October 2006; received in revised form 26 March 2007; accepted 10 July 2007
Available online 24 July 2007

**Abstract**

The electric field and voltage distribution in glass insulators used to support high-voltage lines are very important for their performance. In this paper, a 150 kV glass insulator was simulated. A three-dimensional electric field analysis program has been used for the calculations. The electric field and potential distributions in the vicinity of the insulator was examined. Finally, in order to validate the accuracy of the method, the simulation results were compared to corresponding experimental results with satisfactory agreement. The small deviation between the simulation and the experimental results shows that the simulation methodology is a useful tool for the calculation of the potential in this problem.


*Keywords:* Insulators; Electric field distribution; Voltage distribution; Measurements; Simulation software; Finite element method

## 1. Introduction

Insulators, which are used for the suspension of overhead transmission lines, constitute one of the most important parts of the transmission lines as flashover effects in insulators can cause the breakdown of a transmission network. The calculation of the electric field and potential distribution in and around high voltage insulators is a very important factor in the design of the insulators. In addition, the knowledge of the electric field is useful for the detection of defects in insulators [1].

Considering the complex geometry of the insulators, numerical methods are the preferred method for determining the electric field and potential distribution (EFPD) in the insulator. Numerical methods can be divided into two groups. The first group consists of the charge simulation method and the boundary element method [2]. These two methods are preferable for open boundary problems, such as insulators or power lines. The second group is to solve the governing differential equations. The finite element and finite difference methods are based on differential forms. These two methods are commonly used in the field analysis of problems with limiting boundary conditions, such as rotating machines or transformers [3].

Many different field analysis programs that are based on numerical methods for the field calculation

* Corresponding author. Tel.: +30 2107722226; fax: +30 2107723504.
*E-mail addresses:* vkont@central.ntua.gr (V.T. Kontargyri), igonos@ieee.org (I.F. Gonos).

0263-2241/$ - see front matter © 2007 Elsevier Ltd. All rights reserved.
doi:10.1016/j.measurement.2007.07.002

have been introduced for the simulation of electromagnetic problems. Many simulations have been carried out using these analysis programs in order to calculate the electric field and potential distributions mainly around non-ceramic insulators, because of the highly complicated geometry of ceramic insulators.

The electric field and potential distributions in the vicinity of non-ceramic insulators under dry and clean conditions were presented by Que and Sebo [4]. They used a three-dimensional electric field analysis program based on the boundary element method for the calculations. A three-phase 765 kV power line tower geometry was considered for the potential distribution calculations along the insulators. The effects of the presence of power line conductors and of the three phases versus single phase energization on the electric field and potential distributions were also investigated.

Zhao and Comber applied a two-dimensional and a three-dimensional electric field analysis program to calculate the field distribution of clean and dry non-ceramic insulators [5]. Both analysis programs are based on the boundary element method. A three-phase 345 kV transmission tower with non-ceramic suspension insulators (two I-strings and one V-string) was analyzed. The effects of conductors, tower configurations and grading devices on the electric field and potential distribution along the insulators were investigated. The results quantified the effect of each factor on the electric field and potential distribution.

By using a field probe, Hartings [6] measured the AC electric field along a post insulator under dry and wet conditions and during rain. He discovered that corona activity from the flange carries the potential towards the boundary of the corona region and as a result, the "electrical geometry" of the insulator is modified. The experimental results are consistent with the field calculations based on this new geometry of the insulator. UV photography also supports the findings of the field measurements. Hartings concluded that measuring the electric field distribution with the field probe, in combination with UV photography of the discharge activity, significantly improves the ability to describe and understand the behaviour of outdoor insulators at operating conditions.

A domain decomposition approach for finite-element method calculation of the electric field of insulators applied on high-voltage transmission lines was presented by Sebestyén [7]. This method gives the possibility to examine the effects of various hardware structures, such as line and tower configurations and grading devices, and enables the modeling of very complex geometry without particularly high computational effort. By using this method, the electric stresses acting in and around the insulators are determined, accounting for the interaction of the three-dimensional environment.

## 2. Experimental procedure

The test arrangement that is being used in order to measure the voltage distribution is shown in Fig. 1 [8,9]. It includes a 230 V self-transformer. By this self-transformer, a 110 V/55 kV transformer is fed.

Two methods have been followed in order to measure the voltage. In the first method, a voltmeter in the primary coil of the transformer ($V_1$) is being used. The low voltage $U_1$ is then transformed to high voltage by multiplying the value $U_1$ by the voltage transformer ratio ($a$). In the second method, an electrostatic voltmeter $E_v$ is being used in order to measure the high voltage $U_2$ in the secondary coil of the transformer [8,9]. The average $U_t$ of the two values is the voltage applied across the 10 insulator string:

$$U_{ti} = \frac{U_{1i} \cdot a + U_{2i}}{2} \tag{1}$$

One end of the insulator string (10th insulator) is connected to a transmission line and the other end (1st insulator) is grounded. The first insulator is placed near the tower and the 10th is placed near the transmission line. A sphere-gap is connected in parallel with $i$-insulator. The capacitance of the

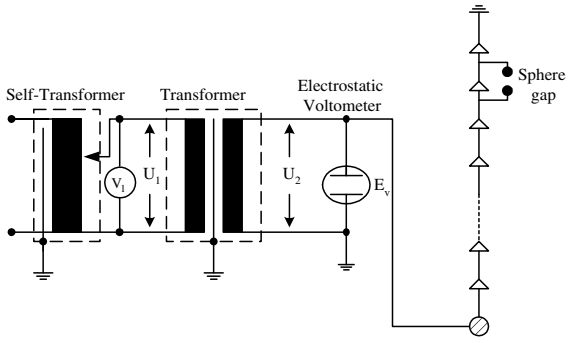


Fig. 1. Experimental set-up used for the measurements of the voltage distribution.

sphere gap is very small compared to the capacitance of the insulator, and thus it can be neglected.

The voltage $U_t$, which is applied to the insulator string, is increased, the critical voltage $U_d$ of the sphere gap is being reached. The percentage of the voltage $P_i$, which is applied to the $i$-insulator, is given by

$$P_i = \frac{U_d}{U_{ti}} \cdot 100\% \quad (2)$$

The existence of the stray capacitances is the reason why the distribution of the voltage in each insulator is not uniform. By positioning the sphere gap in parallel with each of the 10 insulators consecutively and calculating the rates $P_i$ for each insulator, the critical voltage of the sphere gap is calculated by the equation

$$\sum_{i=1}^{10} P_i = U_d \cdot \sum_{i=1}^{10} \frac{1}{U_{ti}} = 1 \quad (3)$$

Fifteen series of measurements have been carried out and the average value and the standard deviation have been calculated. The measurements, which were out of the limits given by Eq. (4), were excluded in order to reduce the measurement error.

$$\mu - 2\sigma < P_i < \mu + 2\sigma \quad (4)$$

where $\mu$ is the average value and $\sigma$ is the standard deviation.

It is noted that the precision of the measurements is proven by the repeatability and reproducibility of the measurement results.

The fieldmeter PMM 8053A and the probe PMM EHP 50B, which are connected via an optic fiber, were used for the calculation of the electric field, as shown in Fig. 2. The probe was placed in different positions on the horizontal plane, while, via the use of successive tubes, measurements were taken in many points of the perpendicular axis.

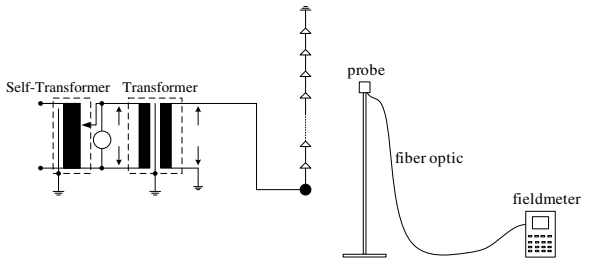


Fig. 2. Experimental set-up used for the measurements of the electric field.

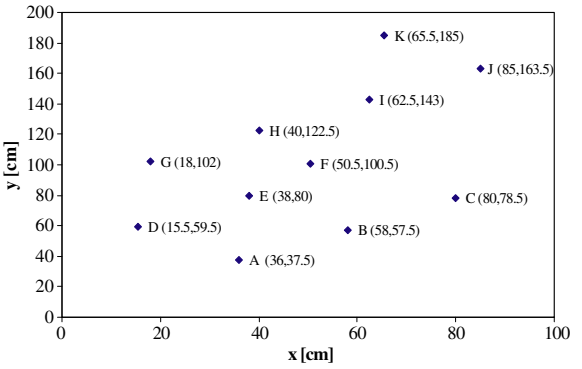


Fig. 3. Locations in the horizontal plane where series of measurements of the electric field were carried out.

The height of the conductor is considered to be the reference point for the measurements. In the horizontal plane the $x$-axis is parallel to the HV conductor and the $y$-axis is perpendicular to the conductor. The point (0, 0) is the point where the $z$-axis (that is the axis of the insulator) intersects the horizontal plane. The electric field was measured at 11 positions on the horizontal plane and at 24 points in each position. In Fig. 3, the coordinates of the 11 positions are shown. The insulator is suspended vertically at the point (0, 0) of the horizontal plane.

## 3. Experimental results

The voltage distribution of the glass insulator string, which is measured using the methodology described in Section 2, is shown in Table 1. The average value $\mu$ of the 15 series of measurements and the standard deviation $\sigma$ have been calculated.

Owing to the stray capacitances existing between the discs and between each disc in the insulator

Table 1
Experimental results of the voltage distribution

| Insulator | Average voltage, $\mu$ (%) | Standard deviation, $\sigma$ (%) |
|---|---|---|
| 1 | 6.57 | 0.11 |
| 2 | 6.21 | 0.03 |
| 3 | 6.29 | 0.09 |
| 4 | 6.66 | 0.12 |
| 5 | 7.60 | 0.11 |
| 6 | 8.69 | 0.04 |
| 7 | 10.55 | 0.29 |
| 8 | 12.33 | 0.21 |
| 9 | 16.00 | 0.13 |
| 10 | 19.16 | 0.11 |

Table 2
Experimental results of the electric field

| $z$ (cm) | Electric field (kV/m) | | | | | | | | | | |
|---|---|---|---|---|---|---|---|---|---|---|---|
| | A | B | C | D | E | F | G | H | I | J | K |
| 0.0 | 15.610 | 9.984 | 6.985 | 10.300 | 6.674 | 4.614 | 4.693 | 3.436 | 2.690 | 2.008 | 1.658 |
| 5.5 | 14.940 | 9.656 | 6.982 | 10.270 | 6.655 | 4.522 | 4.647 | 3.379 | 2.684 | 2.004 | 1.632 |
| 11.0 | 13.970 | 9.289 | 6.667 | 10.000 | 6.612 | 4.473 | 4.617 | 3.404 | 2.667 | 1.978 | 1.615 |
| 16.5 | 12.960 | 8.776 | 6.363 | 9.669 | 6.347 | 4.375 | 4.570 | 3.329 | 2.610 | 1.948 | 1.584 |
| 22.0 | 11.980 | 8.349 | 6.141 | 9.044 | 6.139 | 4.214 | 4.480 | 3.214 | 2.572 | 1.945 | 1.551 |
| 27.5 | 11.340 | 7.752 | 5.921 | 8.969 | 5.968 | 4.044 | 4.355 | 3.169 | 2.523 | 1.924 | 1.533 |
| 33.0 | 10.590 | 7.397 | 5.650 | 8.541 | 5.757 | 3.925 | 4.258 | 3.113 | 2.474 | 1.882 | 1.504 |
| 38.5 | 9.983 | 6.981 | 5.351 | 8.478 | 5.594 | 3.819 | 4.076 | 3.002 | 2.443 | 1.829 | 1.498 |
| 44.0 | 9.230 | 6.669 | 5.115 | 7.964 | 5.356 | 3.754 | 3.968 | 2.912 | 2.371 | 1.774 | 1.459 |
| 49.5 | 8.638 | 6.309 | 4.826 | 7.613 | 5.126 | 3.620 | 3.835 | 2.827 | 2.349 | 1.744 | 1.435 |
| 55.0 | 8.188 | 5.962 | 4.578 | 7.178 | 4.861 | 3.489 | 3.743 | 2.697 | 2.267 | 1.694 | 1.411 |
| 60.5 | 7.572 | 5.627 | 4.267 | 6.812 | 4.615 | 3.313 | 3.578 | 2.605 | 2.146 | 1.664 | 1.369 |
| 66.0 | 7.126 | 5.304 | 4.068 | 6.407 | 4.410 | 3.108 | 3.432 | 2.494 | 2.082 | 1.599 | 1.325 |
| 71.5 | 6.774 | 4.993 | 3.838 | 6.016 | 4.140 | 3.004 | 3.235 | 2.407 | 2.031 | 1.542 | 1.281 |
| 77.0 | 6.313 | 4.748 | 3.663 | 5.670 | 3.939 | 2.910 | 3.122 | 2.319 | 1.935 | 1.508 | 1.231 |
| 82.5 | 5.919 | 4.488 | 3.449 | 5.358 | 3.713 | 2.733 | 2.919 | 2.223 | 1.875 | 1.464 | 1.196 |
| 88.0 | 5.435 | 4.237 | 3.254 | 4.972 | 3.517 | 2.622 | 2.813 | 2.119 | 1.802 | 1.396 | 1.163 |
| 93.5 | 5.163 | 3.978 | 3.091 | 4.747 | 3.305 | 2.450 | 2.640 | 2.031 | 1.705 | 1.327 | 1.129 |
| 99.0 | 4.814 | 3.764 | 2.937 | 4.369 | 3.119 | 2.340 | 2.522 | 1.951 | 1.648 | 1.291 | 1.090 |
| 104.5 | 4.571 | 3.536 | 2.783 | 4.175 | 2.968 | 2.221 | 2.380 | 1.853 | 1.585 | 1.239 | 1.057 |
| 110.0 | 4.287 | 3.266 | 2.623 | 3.853 | 2.821 | 2.111 | 2.246 | 1.789 | 1.508 | 1.205 | 1.027 |
| 115.5 | 3.937 | 3.181 | 2.478 | 3.588 | 2.609 | 2.037 | 2.135 | 1.674 | 1.432 | 1.156 | 0.985 |
| 121.0 | 3.772 | 2.965 | 2.421 | 3.373 | 2.508 | 1.941 | 2.015 | 1.600 | 1.388 | 1.121 | 0.950 |
| 126.5 | 3.423 | 2.757 | 2.274 | 3.167 | 2.373 | 1.852 | 1.897 | 1.508 | 1.319 | 1.057 | 0.918 |

string with respect to the high-voltage conductor as well as to ground , the distribution of the voltage along the insulator is not uniform, the discs nearer the conductor being more highly stressed.

In addition, the three components of the electric field $E_x$, $E_y$ and $E_z$ were measured. The total value of the electric field $E_t$ was calculated according to the following equation

$$E_t = \sqrt{E_x^2 + E_y^2 + E_z^2} \tag{5}$$

The measurements of the electric field at the 11 positions (shown in Fig. 3) around the insulator string are presented in Table 2. Nearer the transmission line, the electric field is higher than farther away from the transmission line.

## 4. Simulation procedure

OPERA-3d (an OPerating environment for Electromagnetic Research and Analysis) [10] is the pre- and post-processing system for the well known electromagnetics analysis programs. Finite element discretisation forms the basis of the methods used in these analysis programs. The post-processor of the Opera-3d provides facilities to view the finite element data, with superimposed contours of results and to process and display the results calculated along lines or on two-dimensional areas.

The analysis presented in this paper was performed using the electromagnetic field analysis program TOSCA electrostatics. The program solves only the Laplace equation:

$$\nabla \cdot \varepsilon \nabla V = 0 \tag{6}$$

The user gives as input to the program the dielectric constant of the materials that are included in the geometry.

A suspension glass insulator 150 kV was simulated. The length of the conductor, that was used for the simulation of the model, was chosen to be equal to the insulator length. The insulator string consists of 10 discs. The geometrical characteristics of the glass insulator are the diameter ($d$), which is 254 mm, the height ($h$), which is 146 mm, and the creepage distance ($L$), which is 290 mm. It is considered that the relative permittivity of the glass and the cement is 7 and 14, respectively.

The value of the electric potential on the surface of the conductor is equal to $150/\sqrt{3}$ kV. In addition, the value of the electric potential on the surfaces of the parallelepiped that simulates the earth

is equal to zero. Equally, the value of the electric potential on the external surfaces of the background is equal to 0 V, as it is assumed that the electric potential in the infinity is zero.

## 5. Simulation results

The model that consists of the insulator string and the transmission line is shown in Fig. 4a. In Fig. 4b a view of an insulator disc is presented in detail.

Two series of graphs are obtained. The first series includes lines that have constant $y = 0$ and the $z$-coordinate gradually increases, which means that the distance from the insulator increases, but the one end of each line is very close to the conductor, as shown in Fig. 5a. The second series includes lines that have constant $x = 0$ and gradually draw away, both from the insulator and the conductor, as shown in Fig. 5b. The potential distribution along lines that have constant $y = 0$ according to the first way of obtaining graphs (Fig. 5a) is shown in Fig. 6.

It is obvious that the potential gradually decreases from the HV electrode $\left(150/\sqrt{3}\,\mathrm{kV}\right)$ towards the grounded electrode (0 V) of the insulator. The blue line ($x = 0$ mm, $y = 0$ mm) in Fig. 6 represents the potential distribution along a line on the interior of the insulator. The rapid reduction of the potential is located at the non-conductive regions of the insulator, and especially at the region of glass. This can be attributed to the low value of the dielectric constant of glass in comparison to this of the other materials that constitute the insulator. The red line ($x = 120$ mm, $y = 0$ mm) represents the potential distribution along a line that touches the outside sheds of the insulator string. The green line ($x = 300$ mm, $y = 0$ mm) and the turquoise line ($x = 600$ mm, $y = 0$ mm) represent the potential distribution along lines that are located 300 mm and 600 mm away from the centre of the insulator, respectively.

The electric-field strength distribution along lines that have constant $x = 0$ (Fig. 5b) is shown in Fig. 7.

The red line ($x = 0$ mm, $y = 120$ mm) in Fig. 7 represents the electric-field strength along a line that touches the outside sheds of the insulator string. The electric field strength along the lines ($x = 120$ mm, $y = 0$ mm) and ($x = 0$ mm, $y = 120$ mm), which touch the outside sheds of the insulator string, goes abruptly down when the line

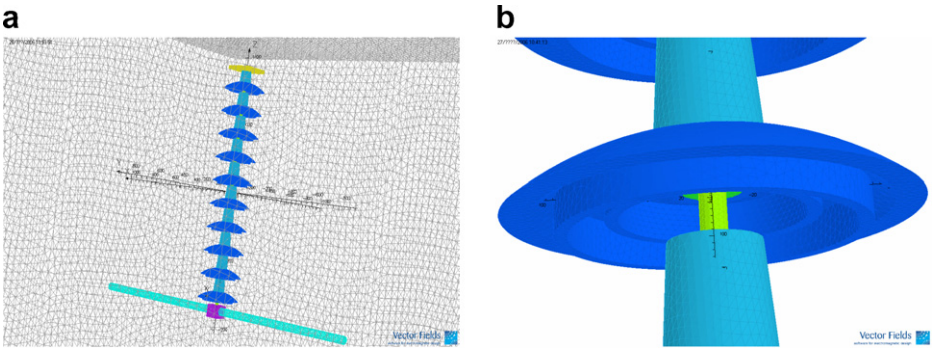


Fig. 4. Views of the model from the post-processor of Opera-3d.

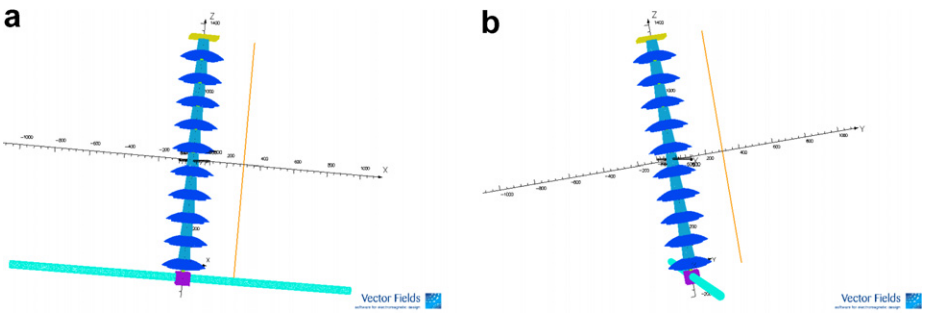


Fig. 5. Presentation of the two ways of obtaining the desirable graphs.

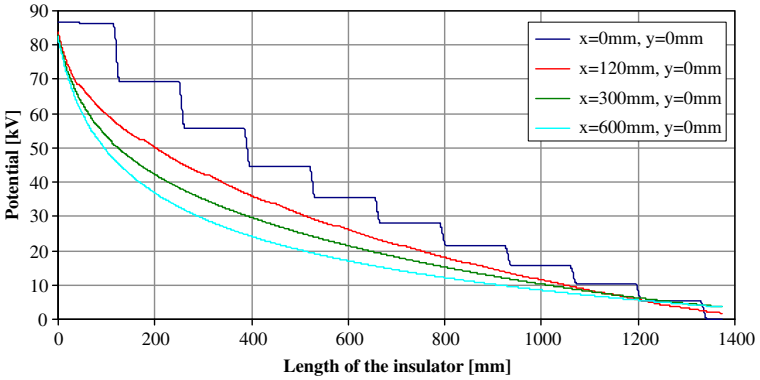


Fig. 6. Comparison of the potential distribution along four different lines parallel to the insulator, according to Fig. 5a.

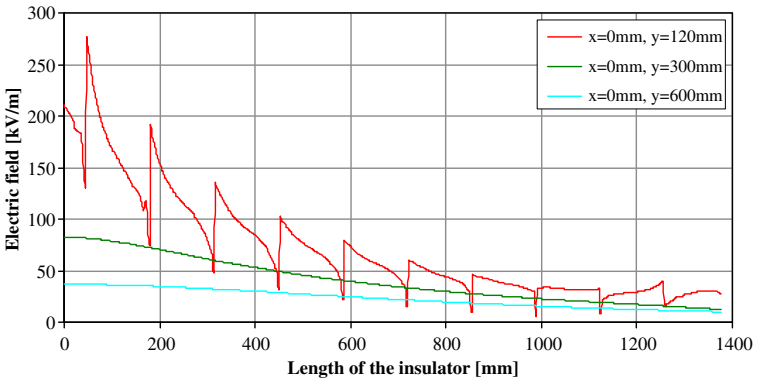


Fig. 7. Comparison of the electric-field strength distribution along three different lines parallel to the insulator, according to Fig. 5b.

goes through the glass sheds. The reason for this is that the value of the dielectric constant of the glass is greater than the dielectric constant of the surrounding air. As a result, there is a significant decrease in the electric field strength at the region of glass. This decrease is also confirmed by [2].

The line ($x = -50, \ldots, 50$ mm, $y = 0$ mm, $z = 50$ mm) that goes through the HV cap is shown in Fig. 8a and the potential distribution along this line is shown in Fig. 8c. The radius of the base of each cap is 35 mm and, as a result, the region $|x| > 35$ mm is covered by air. The pin of the HV insulator is in the region $x = -8.3, \ldots, 8.3$ mm. Due to the conductivity of the pin, the value of the potential in the region of the pin is constant and equals approximately to 86.6 kV, which is the value of the potential that was applied to the conductor. It must be noted that the pin of the HV insulator is connected to the conductor via the purple parallelepiped that is shown in Fig. 4. The first area of cement is located in the region $x = -18.3, \ldots, -8.3$ mm and $x = 8.3, \ldots, 18.3$ mm. The glass is located in the region $x = -27, \ldots, -18.3$ mm and $x = 18.3, \ldots, 27$ mm and the second thin area of cement is located in the region $x = -29, \ldots, -27$ mm and $x = 27, \ldots, 29$ mm. In the above mentioned regions the potential decreases, as is shown in Fig. 8c. Therefore, after the interpolation of the non-conductive regions of the insulator, the value of the potential reaches 70 kV, where it remains constant, as the conductive cap of the HV insulator is located there. The potential reduces almost linearly in the air that surrounds the insulator.

The line ($x = -50, \ldots, 50$ mm, $y = 0$ mm, $z = 1262$ mm) that goes through the grounded cap is shown in Fig. 8b and the potential distribution along this line is shown in Fig. 8d. It is obvious that the maximum potential value (5 kV) is located at the pin of the grounded insulator. The minimum potential value is located at the cap of the grounded insulator, since the cap is grounded.

Below a $yz$-patch is introduced, on which the potential distribution outside and inside the insula-

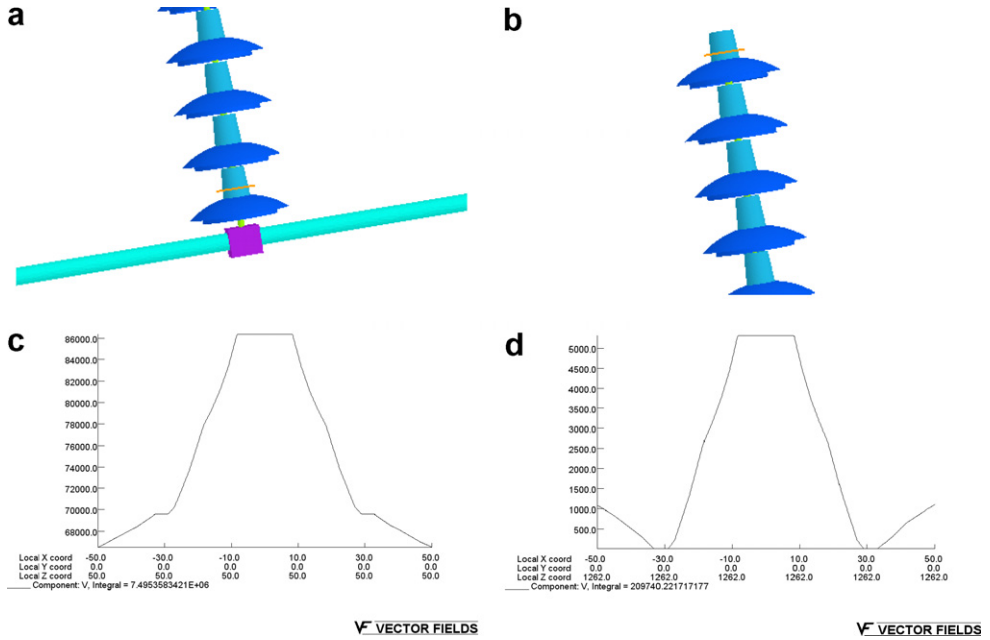


Fig. 8. Potential distribution along a line which is perpendicular to the HV insulator (left) and the grounded insulator (right).

tor string is presented. In Fig. 9, coloured regions around the insulator string represent the potential distribution. It is evident that in a region close to the conductor, the potential is equal to $150/\sqrt{3}$ kV, as expected, and gradually decreases.

The potential distribution in the interior of the insulator string is presented by a histogram in Fig. 10. The potential gradually decreases from the conductor $\left(150/\sqrt{3}\mathrm{kV}\right)$, towards the grounded insulator (0 V). The abrupt reductions (steps) of

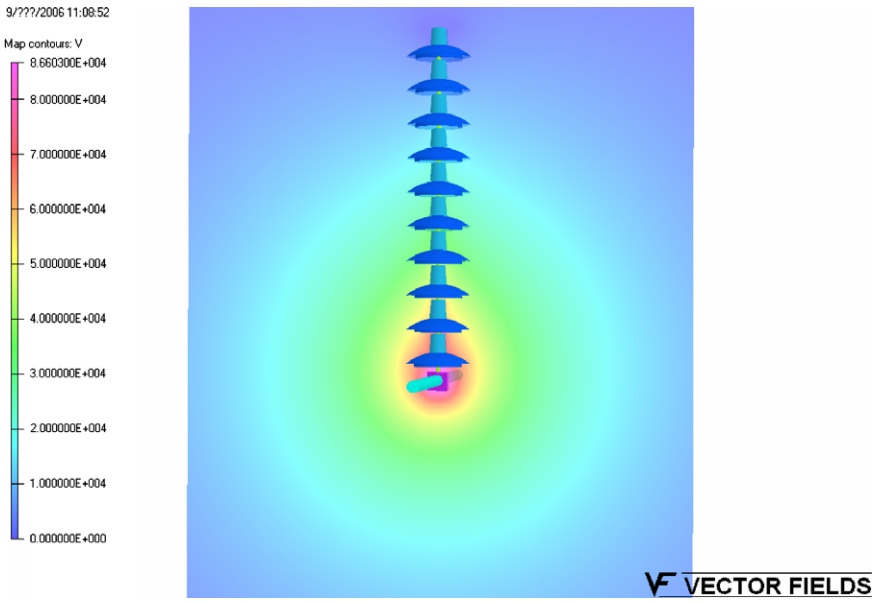


Fig. 9. Zone map on a *yz*-patch for the representation of the potential distribution around the insulator string.

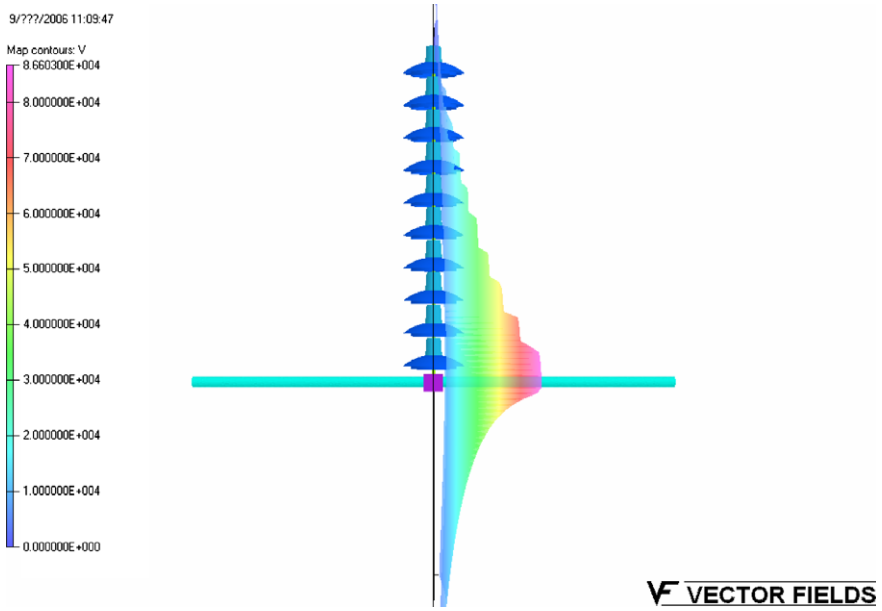


Fig. 10. Histogram on a *yz*-patch for the representation of the potential distribution in the interior of the insulator string.

the potential are located at the non-conductive regions, namely at the regions of cement and, especially, at the region of glass. Besides, it is one of the roles of the insulating material inside an insulator; to cause the gradual decrease of the potential inside the insulator string.

## 6. Comparison between experimental and simulation results

The comparison between experimental and simulation results of the voltage distribution of the glass insulator string is shown in Table 3. It includes the simulation and the experimental results, as well as the error between them.

Table 3
Comparison of the voltage distribution between the simulation and the experimental results

| Insulator | Experimental results (%) | Simulation results (%) | Error (%) |
|---|---|---|---|
| 1 | 6.57 | 6.17 | −6.12 |
| 2 | 6.21 | 5.95 | −4.17 |
| 3 | 6.29 | 6.12 | −2.63 |
| 4 | 6.66 | 6.64 | −0.28 |
| 5 | 7.60 | 7.51 | −1.16 |
| 6 | 8.69 | 8.77 | 0.92 |
| 7 | 10.55 | 10.50 | −0.48 |
| 8 | 12.33 | 12.77 | 3.61 |
| 9 | 16.00 | 15.81 | −1.20 |
| 10 | 19.16 | 19.64 | 2.49 |

Furthermore, the mean square error $m$ was calculated by the equation

$$m = \sqrt{\sum_{i=1}^{N} \left( \frac{1}{N} \left( \frac{P_{si} - P_{ei}}{P_{ei}} \right)^2 \right)} \tag{7}$$

where $P_{si}$ is the value of the percentage of the voltage that is applied on the $i$-insulator acquired by the simulation and $P_{ei}$ is the corresponding experimental value.

It should be noted that the insulator number 1 is the grounded insulator and the insulator number 10 is the HV insulator. The comparison of the voltage distribution between the simulation and the experimental results is shown in Fig. 11. The mean square error $m$ is equal to 2.91.

As can be observed from Fig. 11 the voltage distribution across the insulators is not uniform, owing to the presence of stray capacitances. It is clear from Fig. 11 and Table 3 that the results are very satisfactory, as the mean square error $m$ is 2.91 and the maximum error between the simulation and the experimental results is lower than 6% for each insulator.

In Fig. 12, the electric field simulation results are compared with the experimental results of two indicative positions of the horizontal plane A and G.

The mean square error $m$ for the measurements at the position A is 10.76 and the maximum error between the simulation and the experimental results

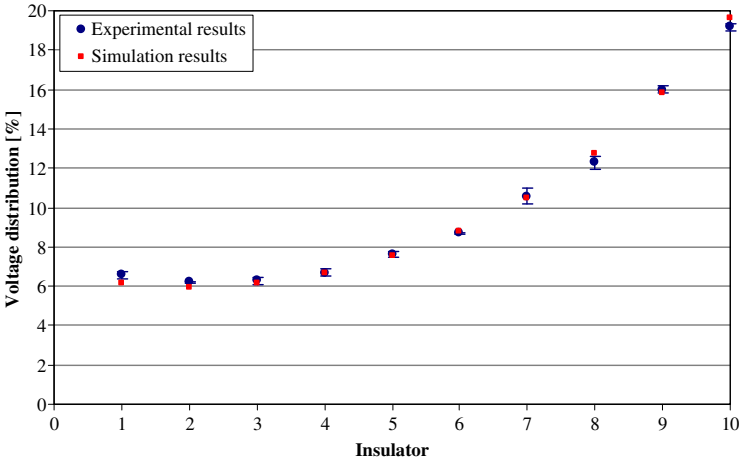


Fig. 11. Comparison of the voltage distribution between the simulation and the experimental results.

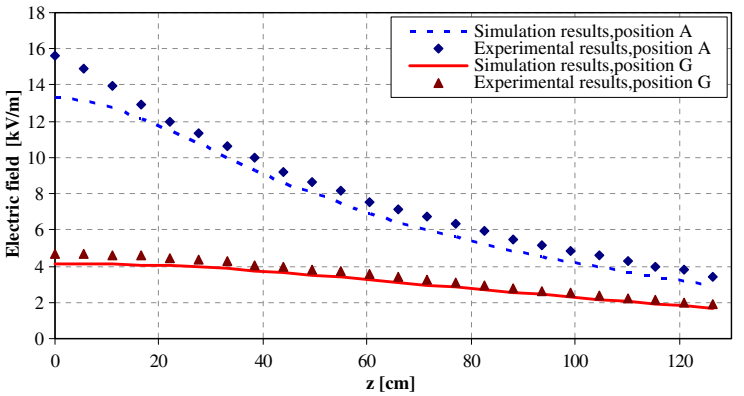


Fig. 12. Comparison of the electric field distribution between the simulation and the experimental results in positions A and G.

is lower than 14%. The mean square error $m$ for the measurements at position G is 9.67 and the maximum error between the simulation and the experimental results is lower than 12%.

## 7. Conclusions and discussion

In this paper, the voltage distribution and the electric field of a glass insulator has been measured and calculated using a program based on the finite elements method. Via this software the electric field and potential distribution can be calculated very easily once the desirable geometry is accurately designed. A very good agreement has been ascertained, when comparing the experimental results with simulated OPERA-3d results. The experimental procedure is a method that gives accurate results due to the repeatability and reproducibility of the measurement values. Taking into account that most of the times the equipment or the place for experiments is not available, the authors propose the use of a simulation program that gives also accurate results in a very fast and economic way.

## Acknowledgements

The authors want to express their sincere gratitude to the Vector Field Company and especially to Dr. A.M. Michaelides for their kind support in the simulations. In addition, this project is co-funded by the European Social Fund (75%) and National Resources (25%) – Operational Program for Educational and Vocational Training II (EPEAEK II) and particularly by the Program HERAKLEITOS.

## References

[1] V.T. Kontargyri, I.F. Gonos, I.A. Stathopulos, A.M. Michaelides, Measurement and verification of the voltage distribution on high-voltage insulators, in: Proceedings of the 12th Biennial IEEE Conference on Electromagnetic Field Computation (CEFC 2006), Maimi, FL, April, 2006.

[2] J.L. Rasolonjanahary, L. Krähenbühl, A. Nicolas, Computation of electric fields and potential on polluted insulators using a boundary element method, IEEE Transactions on Magnetics 38 (2) (1992) 1473–1476.

[3] T. Gustavsson, Outdoor aging of silicone rubber formulations in coastal environment, Licentiate Thesis, Chalmers University of Technology, School of Electrical and Computer Engineering, Göteborg, Sweden, Technical Report No. 353L, 2000.

[4] W. Que, S. Sebo, A Electric Field and Potential Distributions Along Dry and Clean Non-ceramic Insulators. http://www.integratedsoft.com/Papers/research/Coulomb_High_Voltage_paper.pdf.

[5] T. Zhao, G. Comber, Calculation of electric field and potential distribution along non-ceramic insulators considering the effects of conductors and transmission towers, IEEE Transactions on Power Delivery 15 (1) (2000) 313–318.

[6] R. Hartings, Electric fields along a post insulator: AC-measurements and calculations, IEEE Transactions on Power Delivery 9 (2) (1994) 912–918.

[7] I. Sebestyén, Electric-field calculation for HV insulators using domain-decomposition method, IEEE Transactions on Power Delivery 38 (2) (2002) 1213–1216.

[8] IEC 60060-1, High-voltage Test Technique. Part 1. General Definitions and Test Requirements, 1989.

[9] IEC 60060-2, High-voltage Test Technique. Part 2. Measuring Systems, 1994.

[10] Vector Fields, OPERA-3d Reference Manual, Vector Fields Limited, England, 2004.